A hybridizable discontinuous Galerkin method for time-harmonic Maxwell's equations

Stéphane Lanteri, Liang Li, Ronan Perrussel

INRIA

INSTITUT NATIONAL DE RECHERCHE EN INFORMATIQUE ET EN AUTOMATIQUE

A hybridizable discontinuous Galerkin method for time-harmonic Maxwell's equations

S. Lanteri[1], Liang Li[1] and R. Perrussel[2]

[1] : INRIA Sophia Antipolis - Méditerranée research center

[2] : LAPLACE, UMR 5213, CNRS/INPT/UPS

N° 7649

Juin 2011

Rapport de recherche

ISSN 0249-6399 ISRN INRIA/RR--7649--FR+ENG

INSTITUT NATIONAL
DE RECHERCHE
EN INFORMATIQUE
ET EN AUTOMATIQUE

INRIA

centre de recherche
SOPHIA ANTIPOLIS - MÉDITERRANÉE

A hybridizable discontinuous Galerkin method for time-harmonic Maxwell's equations

S. Lanteri[1], Liang Li[1] and R. Perrussel[2]

[1] : INRIA Sophia Antipolis - Méditerranée research center
[2] : LAPLACE, UMR 5213, CNRS/INPT/UPS

Thème : Modélisation, simulation et analyse numérique
Équipe-Projet NACHOS

Rapport de recherche n° 7649 — Juin 2011 — 26 pages

Abstract: In this paper, we study a bybridizable discontinuous Galerkin (HDG) method for the numerical solution of 2D time-harmonic Maxwell's equations. The formulations are given, and the relationship between the HDG scheme and the upwind flux DG method is also examined. The presented numerical results show the effectiveness of the proposed HDG method especially in comparison to the upwind flux DG method.

Key-words: computational electromagnetics, time-harmonic Maxwell's equations, discontinuous Galerkin method, hybridizable method.

Centre de recherche INRIA Sophia Antipolis – Méditerranée
2004, route des Lucioles, BP 93, 06902 Sophia Antipolis Cedex
Téléphone : +33 4 92 38 77 77 — Télécopie : +33 4 92 38 77 65

Une méthode Galerkin discontinue hybride pour les équations de Maxwell en régime harmonique

Résumé : Dans ce rapport, nous étudions une méthode Galerkin discontinue hybride (GDH) pour la résolution des équations de Maxwell en régime harmonique en dimension 2. La formulation est de la méthode GDH est présentée et la relation entre la méthode GDH et la méthode GD basée sur un flux décentré est aussi examinée. Les résultats numériques proposés montrent clairement l'efficacité de la méthode GDH notamment en comparaison à la méthode GD avec un flux décentrée.

Mots-clés : électromagnétisme numérique, méthode Galerkin discontinue, méthode hybride.

1 Introduction

Discontinuous Galerkin (DG) methods have been extensively studied in recent years [ABCM02, CS89, CS98]. This kind of method can be viewed as a clever combination of a finite element method (FEM) and a finite volume method (FVM) [HW08]. A space of basis and test functions is defined as in the FEM on one hand, while the equation is satisfied in a sense closer to the FVM on the other hand. Ideally, the DG methods share almost all the advantages of the FEM and the FVM: adaptivity to complex geometries, easily obtained high-order accuracy, *hp*-adaptivity, add natural parallelism.

The DG methods have been considered for the convection-diffusion equation [CS98], model elliptic equations [ABCM02] and the Helmholtz equation [FW09, FX11]. For Maxwell's equations, DG methods have been developed for both time-domain [HW02, FLLP05, CFP06] and time-harmonic problems [HPS04, HPSS05, DFLP08]. Despite many advantages, the DG methods have one main drawback particularly sensitive for stationnary problems: the number of globally coupled degrees of freedom is $\sum_{i=1}^{N_e} nde_i$ with N_e being the number of elements and nde_i being the number of degrees of freedom on element i, which is *huge* compared to the FEM methods for the same accuracy. Consequently, the DG methods are both CPU time and memory consuming. Hybridization of DG method [CGL09] is devoted to address this issue and keep all the merits of DG methods at the same time.

The hybridizable discontinuous Galerkin (HDG) methods introduce an additional term on the faces of the elements, with which the local solutions can be defined. A so-called *conservativity condition* is imposed on the numerical flux, which can be represented by the additional term, at the interface between neighboring elements. As a result, the HDG methods produce a linear system in terms of the degrees of freedom of the additional hybrid variable only, which greatly reduce the number of globally coupled degrees of freedom. Optimal convergence properties of some HDG methods have been obtained for the convection-diffusion equations [NPC09a, NPC09b] and the Helmholtz equation [GM11] .

We consider a HDG method for solving the time-harmonic Maxwell equations in the present work. In section 2, we introduce the 2D time-harmonic Maxwell equations and the notations. In section 3, the formulation for the HDG method is derived. The discretized formulations based on local polynomial spaces are given in section 4. Section 5 presents some numerical results, which show the optimal convergence order of the HDG methods. The conclusions are drawn in section 6.

2 Problem statement and notations

2.1 Time-harmonic Maxwell's equations in 2D

Time-harmonic Maxwell's equations in 2D without source are considered:

$$\begin{cases} \mathrm{i}\omega\varepsilon_r E - \operatorname{curl}\mathbf{H} = 0, & \text{in } \Omega, \\ \mathrm{i}\omega\mu_r \mathbf{H} + \mathbf{curl}\, E = 0, & \text{in } \Omega, \end{cases} \tag{1}$$

where i is the imaginary unit, ω is the angular frequency, ε_r and μ_r are the relative permittivity and permeability respectively, $E = E_z$ and $\mathbf{H} = \begin{pmatrix} H_x & H_y \end{pmatrix}^T$. The boundary conditions are given by:

$$\begin{cases} E = 0, & \text{on } \Gamma_m, \\ E + (\mathbf{n} \times \mathbf{H}) = E^{\text{inc}} + (\mathbf{n} \times \mathbf{H}^{\text{inc}}) = g^{\text{inc}}, & \text{on } \Gamma_a, \end{cases} \tag{2}$$

with $\Gamma_m \cup \Gamma_a = \partial\Omega$ and $\Gamma_m \cap \Gamma_a = \emptyset$. The first relation of (2) indicates a metallic boundary condition (also called perfect electric conductor condition) on Γ_m, the second relation states a Silver-Müller (first-order absorbing boundary) condition on Γ_a. The operators in this 2D case are:

$$\begin{cases} \mathbf{curl}\, E = \begin{pmatrix} \partial_y E & -\partial_x E \end{pmatrix}^T, \\ \operatorname{curl} \mathbf{H} = \partial_x H_y - \partial_y H_x, \end{cases}$$

and the cross-product of two vectors is $\mathbf{u} \times \mathbf{v} = u_x v_y - u_y v_x$.

2.2 Notations

A triangulation $\mathcal{T}_h$ of Ω is considered.We denote by $\mathcal{F}_h^I$ the union of all interior interfaces (edges in the case of 2D, anyhow, we call it face) of $\mathcal{T}_h$, by $\mathcal{F}_h^B$ the union of all the boundary interfaces of $\mathcal{T}_h$, and by $\mathcal{F}_h = \mathcal{F}_h^I \cup \mathcal{F}_h^B$. Furthermore, $\mathcal{F}_h^B$ is identified to $\partial\Omega$ since we assume that Ω is a polygon. For an interface $F = \overline{K}_1 \cap \overline{K}_2 \in \mathcal{F}_h^I$, let $(\mathbf{v}_i, v_i)$ be the traces of $(\mathbf{v}, v)$ on F from the interior of K_i $(i = 1, 2)$. On this face, we define *mean* (*average*) *values* $\{\cdot\}$ and *jumps* $[\![\cdot]\!]$ as follows:

$$\begin{cases} \{\mathbf{v}\}_F = \dfrac{\mathbf{v}_1 + \mathbf{v}_2}{2}, \\ \{v\}_F = \dfrac{v_1 + v_2}{2}, \\ [\![\mathbf{n} \times \mathbf{v}]\!]_F = \mathbf{n}_{K_1} \times \mathbf{v}_1 + \mathbf{n}_{K_2} \times \mathbf{v}_2, \\ [\![v\mathbf{t}]\!]_F = v_1 \mathbf{t}_{K_1} + v_2 \mathbf{t}_{K_2}. \end{cases}$$

For the boundary faces these expressions are turned to be (assuming $F = \partial K_1 \cap \partial\Omega$):

$$\begin{cases} \{\mathbf{v}\}_F = \mathbf{v}_1, \\ \{v\}_F = v_1, \\ [\![\mathbf{n} \times \mathbf{v}]\!]_F = 0, \\ [\![v\mathbf{t}]\!]_F = \mathbf{0}. \end{cases}$$

Let $\mathbb{P}_p(\omega)$ denote the space of polynomial functions of degree at most p on a domain ω. For any element $K \in \mathcal{T}_h$, let $V^p(K) \equiv \mathbb{P}_p(K)$ and $\mathbf{V}^p(K) \equiv (\mathbb{P}_p(K))^2$. The discontinuous finite element spaces are then introduced by:

$$V_h^p = \left\{ v \in L^2(\Omega) \mid v|_K \in V^p(K),\ \forall K \in \mathcal{T}_h \right\},$$
$$\mathbf{V}_h^p = \left\{ \mathbf{v} \in (L^2(\Omega))^2 \mid \mathbf{v}|_K \in \mathbf{V}^p(K),\ \forall K \in \mathcal{T}_h \right\},$$

where $L^2(\Omega)$ is the space of square integrable functions on the domain Ω. We introduce a traced finite element space which takes into account the metallic boundary condition:

$$M_h^p = \left\{\eta \in L^2(\mathcal{F}_h) \mid \eta|_F \in \mathbb{P}_p(F),\ \forall F \in \mathcal{F}_h \text{ and } \eta|_{\Gamma_m} = 0\right\}. \tag{3}$$

Note that M_h^p consists of functions which are continuous on an edge, but discontinuous at its ends. For two vectorial functions $\mathbf{u}$ and $\mathbf{v}$ in $(L^2(\omega))^2$, we denote $(\mathbf{u},\mathbf{v})_\omega = \int_\omega \mathbf{u}\cdot\mathbf{v}\,\mathrm{d}x$, while for functions u and v in $L^2(\omega)$, we denote $(u,v)_\omega = \int_\omega uv\,\mathrm{d}x$ provided ω is a domain in $\mathbb{R}^2$, and we denote $< u, v >_\omega = \int_\omega uv\,\mathrm{d}s$ if ω is a curve (a section line here). Accordingly, for the triangulation we have:

$$(\cdot,\cdot)_{\mathcal{T}_h} = \sum_{K\in\mathcal{T}_h} (\cdot,\cdot)_K, \qquad < \cdot,\cdot >_{\partial\mathcal{T}_h} = \sum_{K\in\mathcal{T}_h} < \cdot,\cdot >_{\partial K},$$
$$< \cdot,\cdot >_{\mathcal{F}_h} = \sum_{f\in\mathcal{F}_h} < \cdot,\cdot >_F, \qquad < \cdot,\cdot >_{\Gamma_a} = \sum_{f\in\mathcal{F}_h\cap\Gamma_a} < \cdot,\cdot >_F .$$

3 DG and HDG formulations

3.1 Principles

The discontinuous Galerkin method seeks an approximate solution $(E_h, \mathbf{H}_h)$ in the space $V_h^p \times \mathbf{V}_h^p$ satisfying for all K in $\mathcal{T}_h$:

$$\begin{cases} (\mathrm{i}\omega\varepsilon_r E_h, \overline{v})_K - (\operatorname{curl}\mathbf{H}_h, \overline{v})_K = 0,\ \forall v \in V^p(K), \\ (\mathrm{i}\omega\mu_r \mathbf{H}_h, \overline{\mathbf{v}})_K + (\mathbf{curl}\, E_h, \overline{\mathbf{v}})_K = 0,\ \forall \mathbf{v} \in \mathbf{V}^p(K). \end{cases} \tag{4}$$

From integration by parts and by replacing the boundary terms with *numerical traces* $\widehat{E}_h$ and $\widehat{\mathbf{H}}_h$, we have:

$$\begin{cases} (\mathrm{i}\omega\varepsilon_r E_h, \overline{v})_K - (\mathbf{H}_h, \overline{\mathbf{curl}\, v})_K - < \mathbf{n}\times\widehat{\mathbf{H}}_h, \overline{v} >_{\partial K} = 0,\ \forall v \in V^p(K), \\ (\mathrm{i}\omega\mu_r \mathbf{H}_h, \overline{\mathbf{v}})_K + (E_h, \overline{\operatorname{curl}\mathbf{v}})_K - < \widehat{E}_h, \overline{\mathbf{n}\times\mathbf{v}} >_{\partial K} = 0,\ \forall \mathbf{v} \in \mathbf{V}^p(K). \end{cases} \tag{5}$$

In the following, we give a formulation to define $(E_h, \mathbf{H}_h)$ in terms of a hybrid unknown λ_h only. The new variable $\lambda_h \in M_h^p$ is introduced mainly to replace the numerical trace $\widehat{E}_h$ which can now be written as:

$$\widehat{E}_h = \begin{cases} \lambda_h \text{ for } F \in \mathcal{F}_h^I \cup \{\mathcal{F}_h^B \cap \Gamma_a\} \\ 0 \text{ for } F \in \mathcal{F}_h^B \cap \Gamma_m \end{cases} = \lambda_h,\ \forall F \in \mathcal{F}_h. \tag{6}$$

Let $\mathbf{t}$ denote the unitary tangent vector to the face ∂K; then $\mathbf{t}\times\mathbf{n} = 1$ and $\mathbf{v}\times\mathbf{n} = \mathbf{t}\cdot\mathbf{v}$. Here, we consider a numerical trace $\widehat{\mathbf{H}}_h$ of the form:

$$\widehat{\mathbf{H}}_h = \mathbf{H}_h + \tau_K(E_h - \lambda_h)\mathbf{t} \text{ on } \partial K, \tag{7}$$

where τ_K is a local stabilization parameter. Adding the contributions of (5) over all elements and enforcing the continuity of the tangential component of $\widehat{\mathbf{H}}_h$, we can formulate a problem which is to find

$(E_h, \mathbf{H}_h, \lambda_h) \in V_h^p \times \mathbf{V}_h^p \times M_h^p$ such that:

$$\begin{cases} (\mathrm{i}\omega\varepsilon_r E_h, \overline{v})_{\mathcal{T}_h} - (\mathbf{H}_h, \overline{\mathbf{curl}\, v})_{\mathcal{T}_h} - < \mathbf{n} \times \widehat{\mathbf{H}}_h, \overline{v} >_{\partial\mathcal{T}_h} = 0, \ \forall v \in V_h^p, \\ (\mathrm{i}\omega\mu_r \mathbf{H}_h, \overline{\mathbf{v}})_{\mathcal{T}_h} + (E_h, \overline{\mathrm{curl}\, \mathbf{v}})_{\mathcal{T}_h} - < \lambda_h, \overline{\mathbf{n} \times \mathbf{v}} >_{\partial\mathcal{T}_h} = 0, \ \forall \mathbf{v} \in \mathbf{V}_h^p, \\ < [\![\mathbf{n} \times \widehat{\mathbf{H}}_h]\!], \overline{\eta} >_{\mathcal{F}_h} + < \lambda_h, \overline{\eta} >_{\Gamma_a} = < g^{\mathrm{inc}}, \overline{\eta} >_{\Gamma_a}, \ \forall \eta \in M_h^p, \end{cases} \tag{8}$$

where the last equation is called the *conservativity condition*. It also takes the absorbing boundary condition into consideration here. From the expression of $\widehat{\mathbf{H}}_h$ (7), once λ_h is known, we can obtain the local solution through (5) due to the discontinuous nature of V_h^p and $\mathbf{V}_h^p$. Moreover, we can eliminate E_h and $\mathbf{H}_h$ via the first two equations of (8) to obtain a weak formulation in terms of λ_h only. For an interior face $F = \partial K_1 \cap \partial K_2$ we have:

$$\begin{aligned} < [\![\mathbf{n} \times \widehat{\mathbf{H}}_h]\!], \overline{\eta} >_F &= < [\![\mathbf{n} \times (\mathbf{H}_h + \tau(E_h - \lambda_h)\mathbf{t})]\!], \overline{\eta} >_F \\ &= < \mathbf{n}_{K_1} \times \mathbf{H}_1, \overline{\eta} >_{\partial K_1} + < \mathbf{n}_{K_2} \times \mathbf{H}_2, \overline{\eta} >_{\partial K_2} \\ &\quad - < \tau_{K_1} E_1, \overline{\eta} >_{\partial K_1} - < \tau_{K_2} E_2, \overline{\eta} >_{\partial K_2} \\ &\quad + < \tau_{K_1} \lambda_h, \overline{\eta} >_{\partial K_1} + < \tau_{K_2} \lambda_h, \overline{\eta} >_{\partial K_2}, \end{aligned}$$

thus:

$$< [\![\mathbf{n} \times \widehat{\mathbf{H}}_h]\!], \overline{\eta} >_{\mathcal{F}_h} = < \mathbf{n} \times \mathbf{H}_h, \overline{\eta} >_{\partial\mathcal{T}_h} - < \tau E_h, \overline{\eta} >_{\partial\mathcal{T}_h} + < \tau\lambda_h, \overline{\eta} >_{\partial\mathcal{T}_h} . \tag{9}$$

Inserting (9) into (8), we obtain another description of the problem (8) which is to search for the approximation $(E_h, \mathbf{H}_h, \lambda_h) \in V_h^p \times \mathbf{v}_h^p \times M_h^p$ such that:

$$\begin{cases} (\mathrm{i}\omega\varepsilon_r E_h, \overline{v})_{\mathcal{T}_h} - (\mathbf{H}_h, \overline{\mathbf{curl}\, v})_{\mathcal{T}_h} - < \mathbf{n} \times \mathbf{H}_h, \overline{v} >_{\partial\mathcal{T}_h} + < \tau(E_h - \lambda_h), \overline{v} >_{\partial\mathcal{T}_h} = 0, \ \forall v \in V_h^p, \\ (\mathrm{i}\omega\mu_r \mathbf{H}_h, \overline{\mathbf{v}})_{\mathcal{T}_h} + (E_h, \overline{\mathrm{curl}\, \mathbf{v}})_{\mathcal{T}_h} - < \lambda_h, \overline{\mathbf{n} \times \mathbf{v}} >_{\partial\mathcal{T}_h} = 0, \ \forall \mathbf{v} \in \mathbf{V}_h^p, \\ < \mathbf{n} \times \mathbf{H}_h, \overline{\eta} >_{\partial\mathcal{T}_h} - < \tau(E_h - \lambda_h), \overline{\eta} >_{\partial\mathcal{T}_h} + < \lambda_h, \overline{\eta} >_{\Gamma_a} - < g^{\mathrm{inc}}, \overline{\eta} >_{\Gamma_a} = 0, \ \forall \eta \in M_h^p. \end{cases} \tag{10}$$

Integration by parts in the first equation of (10) allows to rewrite this equation as:

$$(\mathrm{i}\omega\varepsilon_r E_h, \overline{v})_{\mathcal{T}_h} - (\mathrm{curl}\, \mathbf{H}_h, \overline{v})_{\mathcal{T}_h} + < \tau(E_h - \lambda_h), \overline{v} >_{\partial\mathcal{T}_h} = 0. \tag{11}$$

The implementation strategy described in section 4 is for problem (10) with the first equation replaced by (11).

3.2 Relationship between HDG and upwind flux DG

The conservativity condition holds on all the interior faces, which means $< [\![\mathbf{n} \times \widehat{\mathbf{H}}]\!], \overline{\eta} >_{\mathcal{F}_h^I} = 0$. From the choice of spaces with p constant, we can infer that $[\![\mathbf{n} \times \widehat{\mathbf{H}}]\!] = 0$ on every interior face on a conforming mesh [CGL09, NPC09a, NPC11]. Substituting $\widehat{\mathbf{H}}$ with the expression in (7), we have:

$$\begin{aligned} [\![\mathbf{n} \times (\mathbf{H}_h + \tau(E_h - \lambda_h)\mathbf{t})]\!] &= [\![\mathbf{n} \times \mathbf{H}_h]\!] - [\![\tau(E_h - \lambda_h)]\!] \\ &= 0 \text{ on } \mathcal{F}_h^I. \end{aligned}$$

For an interior face $F = \partial K_1 \cap \partial K_2$ it holds that:

$$[\![\mathbf{n} \times \mathbf{H}_h]\!] - \tau_{K_1} E_h^1 - \tau_{K_2} E_h^2 + (\tau_{K_1} + \tau_{K_2})\lambda_h = 0 \text{ on } F.$$

Solving for λ_h, we obtain (assuming $\tau_{K_1} + \tau_{K_2} \neq 0$):

$$\widehat{E}_h = \lambda_h = \frac{1}{\tau_{K_1} + \tau_{K_2}}(\tau_{K_1} E_h^1 + \tau_{K_2} E_h^2) - \frac{1}{\tau_{K_1} + \tau_{K_2}}[\![\mathbf{n} \times \mathbf{H}_h]\!] \text{ on } F, \tag{12}$$

recalling the definition of λ_h (6). Inserting the expression for λ_h into the following identity

$$\mathbf{n}_{K_1} \times \widehat{\mathbf{H}}_h^1 = \mathbf{n}_{K_1} \times \mathbf{H}_h^1 + \mathbf{n}_{K_1} \times \tau_{K_1}(E_h^1 - \lambda_h)\mathbf{t}_{K_1},$$

we get:

$$\widehat{\mathbf{H}}_h = \frac{1}{\tau_{K_1} + \tau_{K_2}}(\tau_{K_1} \mathbf{H}_h^1 + \tau_{K_2} \mathbf{H}_h^2) + \frac{\tau_{K_1}\tau_{K_2}}{\tau_{K_1} + \tau_{K_2}}[\![E_h \mathbf{t}]\!] \text{ on } F. \tag{13}$$

The expressions for the numerical fluxes $\widehat{E}_h$ (12) and $\widehat{\mathbf{H}}_h$ (13) suggest a close relationship between the HDG method and the upwind flux DG method. In fact, the proposed HDG method is mathematically equivalent to the upwind flux scheme used in [DFLP08] when the parameter τ is uniformly 1.

4 Implementation

4.1 Local discretization

We first write the local solution $(E_h^\lambda, \mathbf{H}_h^\lambda)$ on K as a function of λ (simplified notation for λ_h). From (10) and (11), we have:

$$\begin{cases} (\mathrm{i}\omega\varepsilon_r E_h^\lambda, \overline{v})_K - (\operatorname{curl} \mathbf{H}_h^\lambda, \overline{v})_K + \tau_K < E_h^\lambda, \overline{v} >_{\partial K} - \tau_K < \lambda, \overline{v} >_{\partial K} = 0, \ \forall v \in V^p(K), \\ (\mathrm{i}\omega\mu_r \mathbf{H}_h^\lambda, \overline{\mathbf{v}})_K + (E_h^\lambda, \overline{\operatorname{curl} \mathbf{v}})_K - < \lambda, \overline{\mathbf{n} \times \mathbf{v}} >_{\partial K} = 0, \ \forall \mathbf{v} \in \mathbf{V}^p(K). \end{cases} \tag{14}$$

For an element K_e, let us write the local solution restricted to K_e as follows:

$$E^e = \sum_{j=1}^{n_p^e} \underline{E}_j^e \varphi_j^e(x, y) \text{ and } \mathbf{H}^e = \begin{pmatrix} H_x^e & H_y^e \end{pmatrix}^T,$$

where n_p^e is the dimension of $\mathbb{P}_p(K_e)$ and φ_j^e's are the local basis functions, with:

$$H_u^e = \sum_{j=1}^{n_p^e} \underline{H}_{uj}^e \varphi_j^e(x, y) \text{ with } u \in \{x, y\},$$

and generally, for a face F_f of the mesh, λ is represented by:

$$\lambda^f = \sum_{j=1}^{n_p^f} \underline{\lambda}_j^f \psi_j^f(x, y),$$

where n_p^f is the dimension of $\mathbb{P}_p(F_f)$ and ψ_j^f's are the local basis functions. After discretization (note that real-valued basis functions are considered), the local linear system resulting from the first equation in (14) is:

$$\mathrm{i}\omega\varepsilon_r\mathbb{M}^e\underline{E}^e + (\mathbb{D}_y^e)^T\underline{H}_x^e - (\mathbb{D}_x^e)^T\underline{H}_y^e + \sum_{l=1}^{3}\tau^{(e,l)}\mathbb{E}^{(e,l)}\underline{E}^e - \sum_{l=1}^{3}\tau^{(e,l)}\mathbb{F}^{(e,l)}\underline{\lambda}^{\sigma(e,l)} = 0, \tag{15}$$

where e is the index of the element of the mesh, (e,l) denotes the face of index l of the element e, $\sigma(e,l)$ maps the local face with index l of the element K_e to its global index, and the entries of the local matrices are defined by:

$$\begin{cases} \mathbb{M}^e[i,j] = \displaystyle\int_{K_e}\varphi_i^e\varphi_j^e\,\mathrm{d}\mathbf{x}, \\ \mathbb{D}_u^e[i,j] = \displaystyle\int_{K_e}(\partial_u\varphi_i^e)\varphi_j^e\,\mathrm{d}\mathbf{x}, \text{ with } u\in\{x,y\}, \\ \mathbb{E}^{(e,l)}[i,j] =< \varphi_j^e, \varphi_i^e >_{\partial K_e^l} = \displaystyle\int_{\partial K_e^l}\varphi_i^e\varphi_j^e\,\mathrm{d}s, \\ \mathbb{F}^{(e,l)}[i,j] =< \psi_j^{\sigma(e,l)}, \varphi_i^e >_{\partial K_e^l} = \displaystyle\int_{\partial K_e^l}\varphi_i^e\psi_j^{\sigma(e,l)}\,\mathrm{d}s, \end{cases}$$

where ∂K_e^l denotes the face of index l of the element K_e. Similarly, the second relation of (14) yields the local systems (we implicitly restrict ourselves to a family of affine elements, mesh is conforming and consists of triangular elements):

$$\begin{cases} \mathrm{i}\omega\mu_r\mathbb{M}^e\underline{H}_x^e - \mathbb{D}_y^e\underline{E}^e + \displaystyle\sum_{l=1}^{3}n_y^{(e,l)}\mathbb{F}^{(e,l)}\underline{\lambda}^{\sigma(e,l)} = 0, \\ \mathrm{i}\omega\mu_r\mathbb{M}^e\underline{H}_y^e + \mathbb{D}_x^e\underline{E}^e - \displaystyle\sum_{l=1}^{3}n_x^{(e,l)}\mathbb{F}^{(e,l)}\underline{\lambda}^{\sigma(e,l)} = 0. \end{cases} \tag{16}$$

From (15) and (16) we can obtain the unknown coefficients of: $\begin{pmatrix}\underline{H}_x^e & \underline{H}_y^e & \underline{E}^e\end{pmatrix}^T$ provided $\underline{\lambda}^{\sigma(e,l)}$, $l = 1,\cdots,3$. The combined local linear system on the element K_e can be written as:

$$\mathbb{A}^e\begin{bmatrix}\underline{H}_x^e\\ \underline{H}_y^e\\ \underline{E}^e\end{bmatrix} + \mathbb{C}^e\begin{bmatrix}\underline{\lambda}^{\sigma(e,1)}\\ \underline{\lambda}^{\sigma(e,2)}\\ \underline{\lambda}^{\sigma(e,3)}\end{bmatrix} = 0, \tag{17}$$

with:

$$\mathbb{A}^e = \begin{bmatrix} \mathrm{i}\omega\mu_r\mathbb{M}^e & 0 & -\mathbb{D}_y^e \\ 0 & \mathrm{i}\omega\mu_r\mathbb{M}^e & \mathbb{D}_x^e \\ (\mathbb{D}_y^e)^T & -(\mathbb{D}_x^e)^T & \mathrm{i}\omega\varepsilon_r\mathbb{M}^e + \displaystyle\sum_{l=1}^{3}\tau^{(e,l)}\mathbb{E}^{(e,l)} \end{bmatrix},$$

and:

$$\mathbb{C}^e = \begin{bmatrix} n_y^{(e,1)}\mathbb{F}^{(e,1)} & n_y^{(e,2)}\mathbb{F}^{(e,2)} & n_y^{(e,3)}\mathbb{F}^{(e,3)} \\ -n_x^{(e,1)}\mathbb{F}^{(e,1)} & -n_x^{(e,2)}\mathbb{F}^{(e,2)} & -n_x^{(e,3)}\mathbb{F}^{(e,3)} \\ -\tau^{(e,1)}\mathbb{F}^{(e,1)} & -\tau^{(e,2)}\mathbb{F}^{(e,2)} & -\tau^{(e,3)}\mathbb{F}^{(e,3)} \end{bmatrix}.$$

4.2 Global discretization for λ

We now consider the discretization form of the third relation of (10) to get a global linear system to solve the unknown coefficient $\underline{\lambda}$. Suppose that the interior face F_f of index f is shared by elements K_e and K_g with local index l and k respectively, *i.e.* $f = \sigma(e,l) = \sigma(g,k)$. For F_f, the conservativity condition (the third relation of (10)) writes as:

$$\begin{aligned} &< \mathbf{n}^{(e,l)} \times \mathbf{H}_h^e, \overline{\eta} >_{\partial K_e^l} + < \mathbf{n}^{(g,k)} \times \mathbf{H}_h^g, \overline{\eta} >_{\partial K_g^k} \\ &\qquad - \tau^{(e,l)} < E_h^e, \overline{\eta} >_{\partial K_e^l} - \tau^{(g,k)} < E_h^g, \overline{\eta} >_{\partial K_g^k} \\ &\qquad + \tau^{(e,l)} < \lambda, \overline{\eta} >_{\partial K_e^l} + \tau^{(g,k)} < \lambda, \overline{\eta} >_{\partial K_g^k} = 0, \ \forall \eta \in V^p(F_f). \end{aligned} \tag{18}$$

The resulting local linear system is:

$$\begin{aligned} &n_x^{(e,l)}(\mathbb{F}^{(e,l)})^T \underline{H}_y^e - n_y^{(e,l)}(\mathbb{F}^{(e,l)})^T \underline{H}_x^e \\ &\qquad - \tau^{(e,l)}(\mathbb{F}^{(e,l)})^T \underline{E}^e + \tau^{(e,l)}\mathbb{G}^{(e,l)}\underline{\lambda}^{\sigma(e,l)} \\ &\qquad + n_x^{(g,k)}(\mathbb{F}^{(g,k)})^T \underline{H}_y^g - n_y^{(g,k)}(\mathbb{F}^{(g,k)})^T \underline{H}_x^g \\ &\qquad - \tau^{(g,k)}(\mathbb{F}^{(g,k)})^T \underline{E}^g + \tau^{(g,k)}\mathbb{G}^{(g,k)}\underline{\lambda}^{\sigma(g,k)} = 0, \end{aligned} \tag{19}$$

where:

$$\mathbb{G}^{(e,l)}[i,j] = < \psi_j^{\sigma(e,l)}, \psi_i^{\sigma(e,l)} > = \int_{\partial K_e^l} \psi_i^{\sigma(e,l)} \psi_j^{\sigma(e,l)} \, \mathrm{d}s.$$

For a boundary face, (19) is replaced by:

$$n_x^{(e,l)}(\mathbb{F}^{(e,l)})^T \underline{H}_y^e - n_y^{(e,l)}(\mathbb{F}^{(e,l)})^T \underline{H}_x^e - \tau^{(e,l)}(\mathbb{F}^{(e,l)})^T \underline{E}^e + (1+\tau^{(e,l)})\mathbb{G}^{(e,l)}\underline{\lambda}^{\sigma,(e,l)} = \underline{g}^{\mathrm{inc},\sigma(e,l)}, \tag{20}$$

where:

$$\underline{g}_i^{\mathrm{inc},\sigma(e,l)} = < g^{\mathrm{inc}}, \psi_i^{\sigma(e,l)} >_{\partial K_e^l} = \int_{\partial K_e^l} g^{\mathrm{inc}} \psi_i^{\sigma(e,l)} \, \mathrm{d}s, \ i = 1, \cdots, n_p^f.$$

From (19), we can write the local system for λ as:

$$\mathbb{B}^e \begin{bmatrix} \underline{H}_x^e \\ \underline{H}_y^e \\ \underline{E}^e \end{bmatrix} + \mathbb{G}^e \begin{bmatrix} \underline{\lambda}^{\sigma(e,1)} \\ \underline{\lambda}^{\sigma(e,2)} \\ \underline{\lambda}^{\sigma(e,3)} \end{bmatrix} + \mathcal{R}^e = 0, \tag{21}$$

where:

$$\mathbb{B}^e = \begin{bmatrix} -n_y^{(e,1)}(\mathbb{F}^{(e,1)})^T & n_x^{(e,1)}(\mathbb{F}^{(e,1)})^T & -\tau^{(e,1)}(\mathbb{F}^{(e,1)})^T \\ -n_y^{(e,2)}(\mathbb{F}^{(e,2)})^T & n_x^{(e,2)}(\mathbb{F}^{(e,2)})^T & -\tau^{(e,2)}(\mathbb{F}^{(e,2)})^T \\ -n_y^{(e,3)}(\mathbb{F}^{(e,3)})^T & n_x^{(e,3)}(\mathbb{F}^{(e,3)})^T & -\tau^{(e,3)}(\mathbb{F}^{(e,3)})^T \end{bmatrix},$$

and:

$$\mathbb{G}^e = \begin{bmatrix} \tau^{(e,1)}\mathbb{G}^{(e,1)} & 0 & 0 \\ 0 & \tau^{(e,2)}\mathbb{G}^{(e,2)} & 0 \\ 0 & 0 & \tau^{(e,3)}\mathbb{G}^{(e,3)} \end{bmatrix},$$

while $\mathcal{R}^e$ gathers the contributions of (19) from the neighboring elements. Note that for a boundary face $\sigma(e,l)$, the corresponding diagonal block of $\mathbb{G}^e$ turns out to be $(1+\tau^{(e,l)})\mathbb{G}^{(e,l)}$, l may be 1, 2 or 3, and the corresponding part of $\mathcal{R}^e$ is replaced by $\underline{g}^{\mathrm{inc},\sigma(e,l)}$, according to (20). Consequently, the global system for λ can be constructed by replacing the coefficients $(\underline{H}_x^e, \underline{H}_y^e, \underline{E}^e)$ with their local solution from (17). To get an explicit formulation, let us give some notations. Let $N_\lambda^{(e,l)}$ denote the number of degrees of freedom of λ on the face with local index l of element K_e (the element with index e), N_λ denotes the total number of degrees of freedom of λ and let:

$$\tilde{N}_\lambda = \sum_{e=1}^{N_e} \sum_{l=1}^{3} N_\lambda^{(e,l)},$$

where N_e is the number of elements of $\mathcal{T}_h$. We then introduce the trace space spreading operator $\mathcal{A}_{HDG}$ as a matrix of size $\tilde{N}_\lambda \times N_\lambda$ which *scatters* the unique trace space values to their local edge vectors [KSC10]. The matrix $\mathcal{A}_{HDG}$ can be organized as:

$$\mathcal{A}_{HDG} = \begin{bmatrix} \mathcal{A}_{HDG}^1 \\ \vdots \\ \mathcal{A}_{HDG}^{N_e} \end{bmatrix},$$

where the action of $\mathcal{A}_{HDG}^e$ is to copy the global trace space information into local (element-wise) storage. With these notations, we can rewrite the equation for the local solver (17) as:

$$\mathbb{A}^e \underline{W}^e + \mathbb{C}\mathcal{A}_{HDG}^e \underline{\Lambda} = 0, \tag{22}$$

where $\underline{W}^e = \begin{pmatrix} \underline{H}_x^e & \underline{H}_y^e & \underline{E}^e \end{pmatrix}^T$ and $\underline{\Lambda}$ is the vector gathering all the global trace space information. Adding all the equations involving every interior face (19) and every boundary face (20) element by element we have:

$$\sum_{e=1}^{N_e} (\mathcal{A}_{HDG}^e)^T [\mathbb{B}^e \underline{W}^e + \mathbb{G}^e \mathcal{A}_{HDG}^e \underline{\Lambda}] = \sum_{e=1}^{N_e} (\mathcal{A}_{HDG}^e)^T \underline{g}^e \equiv \underline{g},$$

where the sum over elements along with the left application of the transpose of $\mathcal{A}_{HDG}^e$ allows to gather the element-wise contributions corresponding to face and:

$$\underline{g}^e = \begin{bmatrix} \underline{g}^{\mathrm{inc},\sigma(e,1)} & \underline{g}^{\mathrm{inc},\sigma(e,2)} & \underline{g}^{\mathrm{inc},\sigma(e,3)} \end{bmatrix}^T,$$

$\underline{g}^{\mathrm{inc},\sigma(e,l)}$ $(l = 1,2,3)$ is non trivial only on the faces lying on the boundary Γ_a. Replacing $\underline{W}^e$ with its solution from the local system (22), we get:

$$\sum_{e=1}^{N_e} (\mathcal{A}_{HDG}^e)^T [-\mathbb{B}^e (\mathbb{A}^e)^{-1} \mathbb{C}^e \mathcal{A}_{HDG}^e \underline{\Lambda} + \mathbb{G}^e \mathcal{A}_{HDG}^e \underline{\Lambda}] = \underline{g}, \tag{23}$$

with which we can obtain a global equation for $\underline{\Lambda}$:

$$\mathbf{K}\underline{\Lambda} = \underline{g}, \tag{24}$$

where:

$$\mathbf{K} = \sum_{e=1}^{N_e} (\mathcal{A}_{HDG}^e)^T \mathbb{K}^e \mathcal{A}_{HDG}^e = \sum_{e=1}^{N_e} (\mathcal{A}_{HDG}^e)^T [\mathbb{G}^e - \mathbb{B}^e (\mathbb{A}^e)^{-1} \mathbb{C}^e] \mathcal{A}_{HDG}^e.$$

Thus, the assembly of (24) can be performed as a classical FE assembly process with a sequence of computations of elementary matrices $\mathbb{K}^e$.

4.3 Well-posedness of the local solver

In (14), we consider $v = E_h^\lambda$ and $\mathbf{v} = \mathbf{H}_h^\lambda$ and, by adding the two relations together, we obtain:

$$\begin{aligned}(\mathrm{i}\omega\varepsilon_r E_h^\lambda, \overline{E_h^\lambda})_K - (\operatorname{curl}\mathbf{H}_h^\lambda, \overline{E_h^\lambda})_K + \tau_K < (E_h^\lambda - \lambda), \overline{E_h^\lambda} >_{\partial K} + \\ (\mathrm{i}\omega\mu_r \mathbf{H}_h^\lambda, \overline{\mathbf{H}_h^\lambda})_K + (E_h^\lambda, \overline{\operatorname{curl}\mathbf{H}_h^\lambda})_K - \tau_K < \lambda, \overline{E_h^\lambda} >_{\partial K} = 0.\end{aligned}$$

Taking $\lambda = 0$, it results in the following equality:

$$(\mathrm{i}\omega\varepsilon_r E_h^\lambda, \overline{E_h^\lambda})_K + (\mathrm{i}\omega\mu_r \mathbf{H}_h^\lambda, \overline{\mathbf{H}_h^\lambda})_K + 2\Im((E_h^\lambda, \overline{\operatorname{curl}\mathbf{H}_h^\lambda})_K) + \tau_K < E_h^\lambda, \overline{E_h^\lambda} >_{\partial K} = 0. \tag{25}$$

We cannot conclude on the general well-posedness of the local solver because it is possible to have resonant frequencies in the relation (25). However, this problem never showed up in our experiments. In the following sections, we always assume that the local solver is well-posed. Considering the real part of (25), we have $\tau_K < E_h^\lambda, \overline{E_h^\lambda} >_{\partial K} = 0$ (both ε_r and μ_r are real numbers), which implies that $E_h^\lambda = 0$ on ∂K. In the HDG-P1 case (i.e., $n_p^e = 3$ and $n_p^f = 2$), all the degrees of freedom are on ∂K, thus $E_h^\lambda = 0$ on the entire element K. Thus $\mathbf{H}_h^\lambda = 0$ on K, by the comparison of the imaginary parts of (25) on both sides. As a result, we can assure at least the well-posedness of the local solver for the HDG-P1 method. This is coherent with the results stated in [FX11].

4.4 Characterization of the reduced system

We explicitly rewrite the reduced system:

$$a_h(\lambda_h, \eta) = b_h(\eta), \ \forall \eta \in M_h^p, \tag{26}$$

with:

$$\begin{aligned} a_h(\lambda_h, \eta) &= < [\![\mathbf{n} \times \widehat{\mathbf{H}}_h^\lambda]\!], \overline{\eta} >_{\mathcal{F}_h} + < \lambda, \overline{\eta} >_{\Gamma_a}, \\ b_h(\eta) &= < g^{\mathrm{inc}}, \overline{\eta} >_{\Gamma_a}, \end{aligned}$$

where the subscript h of λ is taken out for simplicity. In the following, we are going to explore the properties of the sesquilinear form $a_h(\lambda_h, \eta)$. For any $\eta \in M_h^p$, we denote the solution by $(E_h^\eta, \mathbf{H}_h^\eta)$ whose

restriction to an element K of $\mathcal{T}_h$ is the solution of the local problem:

$$\begin{cases} (\mathrm{i}\omega\varepsilon_r E_h^\eta, \overline{v})_K - (\mathrm{curl}\,\mathbf{H}_h^\eta, \overline{v})_K - < \mathbf{n}\times(\widehat{\mathbf{H}}_h^\eta - \mathbf{H}_h^\eta), \overline{v} >_{\partial K} = 0, \ \forall v \in V^p(K), \\ (\mathrm{i}\omega\mu_r \mathbf{H}_h^\eta, \overline{\mathbf{v}})_K + (E_h^\eta, \overline{\mathrm{curl}\,\mathbf{v}})_K - < \eta, \overline{\mathbf{n}\times\mathbf{v}} >_{\partial K} = 0, \ \forall \mathbf{v} \in \mathbf{V}^p(K), \end{cases} \tag{27}$$

which are the formulations we used in the implementation. Summing the contributions over all the elements of $\mathcal{T}_h$, we obtain the following formulations by recalling the definition of $[\![\cdot]\!]$:

$$\begin{cases} (\mathrm{i}\omega\varepsilon_r E_h^\eta, \overline{v})_{\mathcal{T}_h} - (\mathrm{curl}\,\mathbf{H}_h^\eta, \overline{v})_{\mathcal{T}_h} - < [\![\mathbf{n}\times(\widehat{\mathbf{H}}_h^\eta - \mathbf{H}_h^\eta)]\!], \overline{v} >_{\mathcal{F}_h} = 0, \ \forall v \in V_h^p, \\ (-\mathrm{i}\omega\mu_r \overline{\mathbf{H}_h^\eta}, \mathbf{v})_{\mathcal{T}_h} + (\overline{E_h^\eta}, \mathrm{curl}\,\mathbf{v})_{\mathcal{T}_h} - < \overline{\eta}, [\![\mathbf{n}\times\mathbf{v}]\!] >_{\mathcal{F}_h} = 0, \ \forall \mathbf{v} \in \mathbf{V}_h^p. \end{cases} \tag{28}$$

Note that the second relation of (28) is got by taking the summation in the complex conjugate of the second relation of (27). The sequilinear form in (26) can now be obtained:

$$\begin{aligned} a_h(\lambda_h, \eta) &= < [\![\mathbf{n}\times\widehat{\mathbf{H}}_h^\lambda]\!], \overline{\eta} >_{\mathcal{F}_h} + < \lambda, \overline{\eta} >_{\Gamma_a} \\ &= < [\![\mathbf{n}\times\mathbf{H}_h^\lambda]\!], \overline{\eta} >_{\mathcal{F}_h} + < [\![\mathbf{n}\times(\widehat{\mathbf{H}}_h^\lambda - \mathbf{H}_h^\lambda)]\!], \overline{\eta} >_{\mathcal{F}_h} + < \lambda, \overline{\eta} >_{\Gamma_a} \\ &= (-\mathrm{i}\omega\mu_r \overline{\mathbf{H}_h^\eta}, \mathbf{H}_h^\lambda)_{\mathcal{T}_h} + (\overline{E_h^\eta}, \mathrm{curl}\,\mathbf{H}_h^\lambda)_{\mathcal{T}_h} + < [\![\mathbf{n}\times(\widehat{\mathbf{H}}_h^\lambda - \mathbf{H}_h^\lambda)]\!], \overline{\eta} >_{\mathcal{F}_h} + < \lambda, \overline{\eta} >_{\Gamma_a} \\ &\quad \text{(by the second relation of (28), taking } \mathbf{v} = \mathbf{H}_h^\lambda) \\ &= (-\mathrm{i}\omega\mu_r \overline{\mathbf{H}_h^\eta}, \mathbf{H}_h^\lambda)_{\mathcal{T}_h} + (\mathrm{i}\omega\varepsilon_r E_h^\lambda, \overline{E_h^\eta})_{\mathcal{T}_h} + < [\![\mathbf{n}\times(\widehat{\mathbf{H}}_h^\lambda - \mathbf{H}_h^\lambda)]\!], (\overline{\eta} - \overline{E_h^\eta}) >_{\mathcal{F}_h} + < \lambda, \overline{\eta} >_{\Gamma_a} \\ &\quad \text{(by the first relation of (28)).} \end{aligned}$$

Considering the definition of $\widehat{\mathbf{H}}_h^\lambda$ (7), we have:

$$a_h(\lambda_h, \eta) = (-\mathrm{i}\omega\mu_r \mathbf{H}_h^\lambda, \overline{\mathbf{H}_h^\eta})_{\mathcal{T}_h} + (\mathrm{i}\omega\varepsilon_r E_h^\lambda, \overline{E_h^\eta})_{\mathcal{T}_h} + < \tau(\lambda - E_h^\lambda), \overline{(\eta - E_h^\eta)} >_{\partial\mathcal{T}_h} + < \lambda, \overline{\eta} >_{\Gamma_a}. \tag{29}$$

When ε_r and μ_r are real-valued, we can infer that the coefficient matrix $\mathbf{K}$ in (24) is complex symmetric and all the eigenvalues lie in the right half-plane of the complex plane, because we use real-valued basis functions. Moreover, the first two terms define the imaginary part of $\mathbf{K}$ if ε_r, μ_r and the basis functions are real-valued. This matrix part is similar to the discretization of the wave equation : it is symmetric but indefinite as soon as ω is sufficiently large (this point will be assessed in the numerical experiments).

5 Numerical results

In this section, we provide some numerical results to show the effectiveness of the proposed HDG method. The DG and HDG methods have been implemented in Fortran 90 and run on an HP Z400 workstation with an Intel (R) Xeon (R) CPU and 4 GB of RAM. Two simple problems are considered in order to evaluate the method.

5.1 Plane wave propagation in vacuum

We first consider the propagation of a plane wave in vacuum. The computational domain is chosen to be the unit square $\Omega =]0;1[^2$, and the Silver Müller absorbing boundary condition is imposed on the whole

boundary. The electromagnetic parameters ε_r and μ_r are set to be 1 everywhere, and unless otherwise stated the angular frequency is $\omega = 4\pi$ and $\tau = 1$ in the HDG formulation. Our implementation of the high order DG and HDG methods makes use of nodal basis functions with equispaced nodes up to order 4.

5.1.1 Structured triangular meshes

Structured triangular meshes are considered in this subsection. We tested both the upwind flux based DG method and the HDG method. The numerical convergence results in a logarithmic scale are presented in Figure 1. Compared to the upwind flux based DG method, the HDG method can achieve the same accuracy but with less degrees of freedom (DOF). In fact, for 2D Maxwell's equations, the number of unknowns of the HDG method is $N_{HDG} = N_f \cdot ndf$, with N_f the number of faces (edges in the case of 2D), and ndf the number of DOFs on each face, while, the number of unknowns of the upwind flux based DG scheme is $N_{UP} = 3N_e \cdot nde$, with N_e the number of elements (triangles in this case), nde the number of DOFs on each element. Approximately, $N_f = \frac{3}{2}N_e$, and $ndf = p + 1$, $nde = \frac{(p+1)(p+2)}{2}$, so with the increase of the degree of the interpolation polynomial, the reduction of the number of DOFs by the HDG method can be seen more and more evidently. We can also observe from Figure 1 the interest of higher order polynomial approximations which allows a considerable reduction of the number of DOFs. A detailed comparison between the HDG method and the upwind flux based DG method is given in Table 1. And the numerically estimated convergence order (using a linear regression method) of the HDG method is given in Table 2.

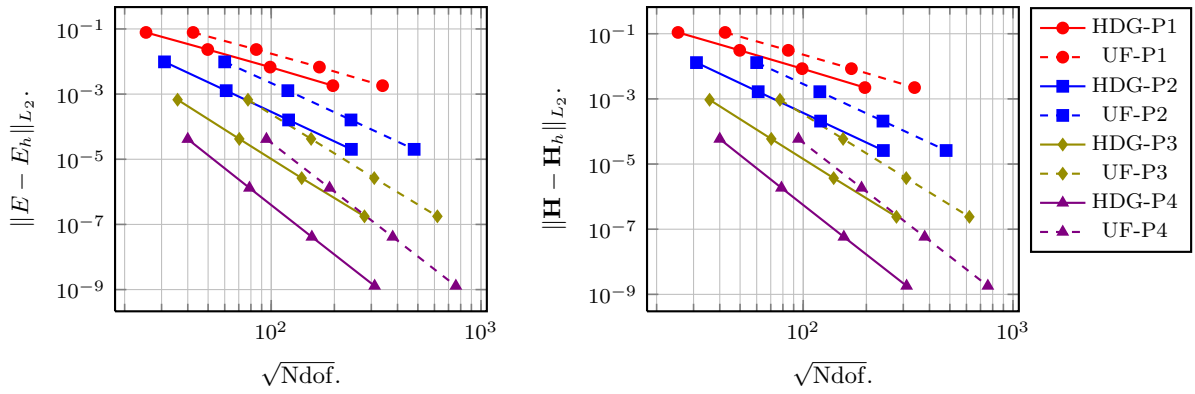

Figure 1: L_2-error for both E and $\mathbf{H}$ fields for several polynomial approximations. Ndof is the number of degrees of freedom. HDG-Pi and UF-Pi , $i = 1, 2, 3, 4$ refer to the convergence plots for the HDG and upwind flux based DG methof respectively.

In Table 1, "MS" denotes the mesh size, "Memory" denotes the memory occupancy in MB when solving the global linear system by the MUMPS sparse direct solver, "$T_{\text{construction}}$" denotes the CPU time in seconds for the construction of the global linear system and "T_{solution}" denotes the CPU time is seconds

for solving the resulting linear system. From the results in Table 1, we note that the HDG method

Table 1: Comparisons between HDG and upwind flux scheme on memory and CPU time.

MS	Memory		$T_{\text{construction}}$		T_{solution}	
	HDG	upwind	HDG	upwind	HDG	upwind
			P1			
0.14	2	5	0.00	0.00	0.01	0.03
0.071	5	19	0.01	0.00	0.02	0.10
0.035	20	85	0.03	0.01	0.04	0.64
0.018	86	389	0.09	0.03	0.52	3.87
			P2			
0.14	3	11	0.01	0.00	0.01	0.07
0.071	9	48	0.03	0.01	0.04	0.35
0.035	41	221	0.09	0.02	0.22	2.06
0.018	187	1024	0.37	0.08	1.27	13.33
			P3			
0.14	4	21	0.02	0.01	0.01	0.14
0.071	15	96	0.08	0.02	0.08	0.77
0.035	71	435	0.29	0.05	0.29	4.63
0.018	327	1955	1.16	0.19	2.54	31.14
			P4			
0.14	5	36	0.05	0.01	0.02	0.30
0.071	24	160	0.21	0.03	0.12	1.45
0.035	106	720	0.80	0.11	0.67	8.29
0.018	499	3258	3.17	0.40	4.54	51.41

requires less memory cost as well as the CPU time for a given target accuracy as compared to the DG metho. The CPU time for the construction of the global matrix of the HDG method is higher than that of the upwind flux DG method, because in the HDG method we are required to compute $\mathbb{K}^e = \mathbb{B}^e(\mathbb{A}^e)^{-1}\mathbb{C}^e$ on each element. Note that it is not necessary to explicitly compute the entries of $(\mathbb{A}^e)^{-1}$, and the computation of $\mathbb{K}^e$ for each element is parallel, which means the construction time can be reduced in a parallel implementation of the method. However the CPU time for solving the global linear system and the total CPU time consumed by the HDG method are much less than those of the upwind flux based DG method due to a drastic reduction of number of globally coupled unknowns. In order to study how the parameter τ affects the convergence of the HDG method, we give the errors of both E field and $\mathbf{H}$ field versus different values of τ in Figure 2. The results are obtained using the HDG-P3 scheme and the angular frequency is set to be $\omega = 4\pi$ and the mesh size is 0.071. Figure 2 shows that the convergence of the HDG method is not so sensitive to the choice of τ. The condition numbers of the coefficient matrices of the resulting global linear systems are presented in Figure 3. The results for the HDG-P1

Table 2: Numerical convergence order of the HDG method.

	P1	P2	P3	P4
E field	1.8	3.0	4.0	5.0
$\mathbf{H}$ field	1.9	3.0	4.0	5.0

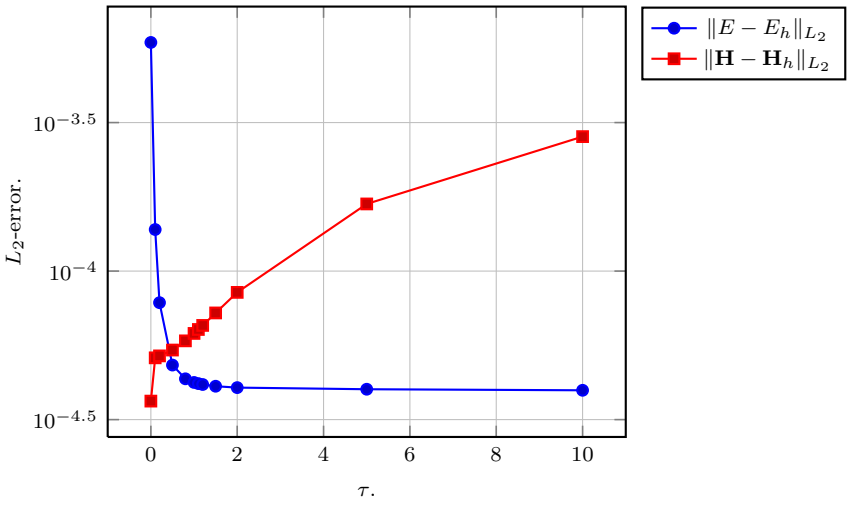

Figure 2: Errors of both E and $\mathbf{H}$ field versus τ.

and HDG-P3 methods are given here, but we observed similar behaviors for the HDG-P2 and HDG-P4 methods. We find that the condition numbers decrease as the frequency of the incident wave grows. The condition number is more dependent on the mesh size and the size of the matrix. This provides a good chance to develop efficient iterative solvers for the resulting linear systems. A similar conclusion has also been made by Griesmaier and Monk in [GM11], where a HDG method is studied for the solution of the Helmholtz equation. The distributions of the eigenvalues of the global matrix $\mathbf{K}$ of (24) for the coarsest

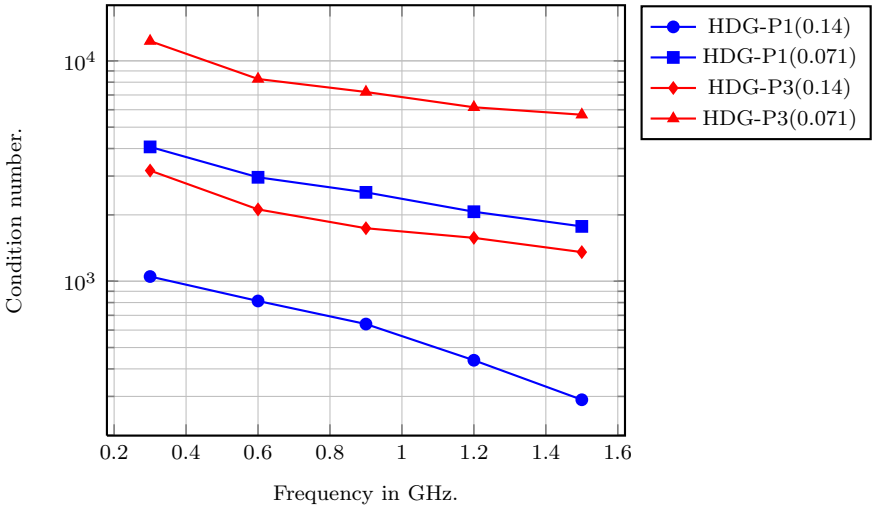

Figure 3: Condition numbers versus frequency. The mesh sizes are provided in the parentheses.

mesh, *i.e.* $h = 0.14$, are shown in Figure 4. All the eigenvalues have non-negative (positive in this case) real parts, which is in agreement with the conclusion made in subsection 4.4. From Figure 4, we can also find that on the same mesh the eigenvalues become clustered as the frequency increases, which agrees with the observation from Figure 3. Finally, it can be noticed that the number of eigenvalues with a positive imaginary part increases when ω increases for a fixed discretization; this is due to the indefinite and wave equation like nature of the imaginry part of the matrix as underlined in subsection 4.4.

5.1.2 Unstructured triangular meshes

Independently refined unstructured triangular meshes are used in this subsection. Four meshes are involved, and the mesh sizes are 0.184, 0.123, 0.0578 and 0.0289, respectively. The first three meshes are shown in Figure 5. Numerical convergence results are plotted in Figure 6. The estimated numerical convergence orders are given in Table 3.

In summary, optimal convergence orders are obtained for both E and $\mathbf{H}$ fields on structured or unstructured meshes, concluded from Figure 1, Figure 6, Table 2 and Table 3.

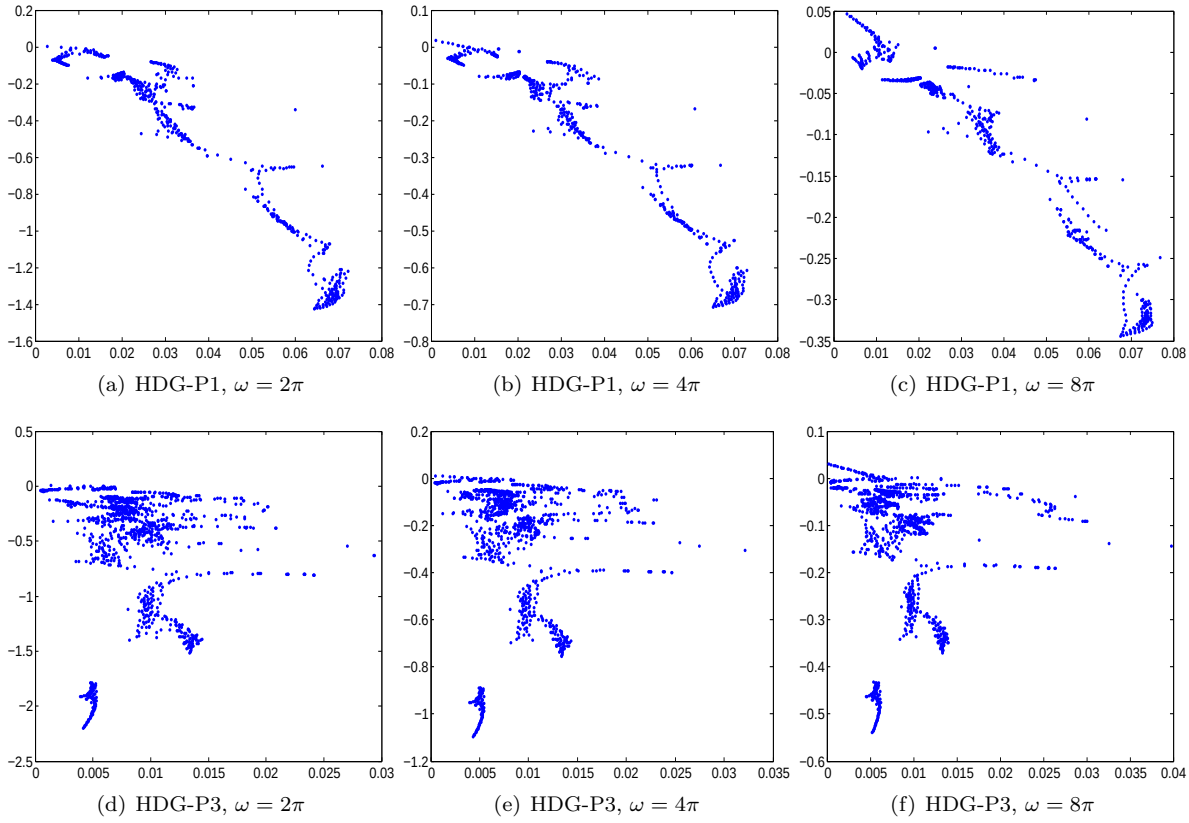

(a) HDG-P1, $\omega = 2\pi$ (b) HDG-P1, $\omega = 4\pi$ (c) HDG-P1, $\omega = 8\pi$

(d) HDG-P3, $\omega = 2\pi$ (e) HDG-P3, $\omega = 4\pi$ (f) HDG-P3, $\omega = 8\pi$

Figure 4: Distributions of the eigenvalues of the global matrix for different values of the incident wave frequency.

Table 3: Numerical convergence order using the HDG method on independent unstructured triangular meshes.

	P1	P2	P3	P4
E field	2.0	3.1	4.2	5.2
$\mathbf{H}$ field	2.0	3.1	4.2	5.2

5.2 Scattering of a metallic cylinder

Electromagnetic scattering of an infinite metallic cylinder is considered. The radius of the cylinder is taken to be λ_0, where λ_0 denotes the wavelength of the incident wave in the vacuum. The artificial absorbing boundary is set to be a concentric circle with radius being $3\lambda_0$. The angular frequency is

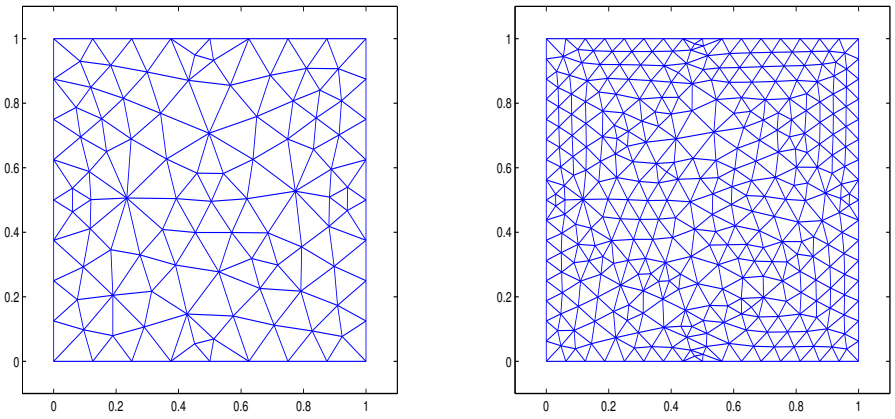

(a) $h = 0.184$ (b) $h = 0.123$

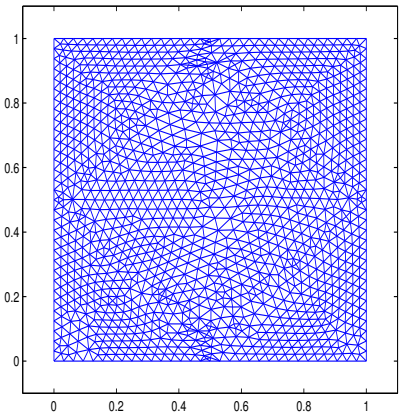

(c) $h = 0.0578$

Figure 5: Unstructured triangular meshes.

$\omega = 2\pi$, which implies that the radius of the cylinder is one. We use five independently refined meshes, with mesh size: 0.660, 0.372, 0.257, 0.191, 0.0960, respectively. The first three meshes are shown in Figure 7.

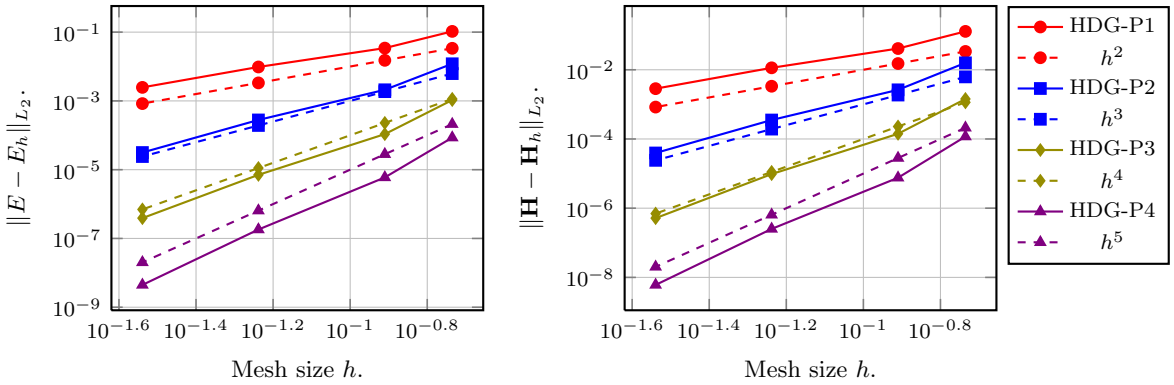

Figure 6: Convergence results of both E and $\mathbf{H}$ fields on independent unstructured triangular meshes.

The contour lines of the E_z as well as the H_x components are shown on Figures 8 and 9. Numerical convergence results in a logarithmic scale are shown in Figure 10. Numerical convergence orders for the HDG-P1 and HDG-P2 schemes are summarized in Table 4.

Table 4: Numerical convergence order of the HDG method for the scattering by a metaalic cylinder problem.

Method	HDG-P1		HDG-P2	
Field	E field	$\mathbf{H}$ field	E field	$\mathbf{H}$ field
Convergence order	2.2	2.1	2.4	2.4

The optimal convergence order of the HDG-P1 method is also obtained for both E and $\mathbf{H}$ fields. However, the convergence order of the HDG-P2 method is no longer 3, because the geometric error dominates due to the discertization of the curved boundaries by affine elements [Fah10]. Some isoparametric maps have to be studied to make use of higher order schemes.

6 Conclusion

We studied a HDG method for the solution of the 2D time-harmonic Maxwell's equations. Compared to the former DG methods, the HDG method can save much computing time and memory cost to reach the same accuracy. The convergence order of the HDG method is numerically proved to be optimal. However, we are still at the beginning point of solving more realistic electromagnetic problems by the HDG method. There are several aspects to be studied: non affine element family, stability analysis, 3D problems, parallel implementation, etc.

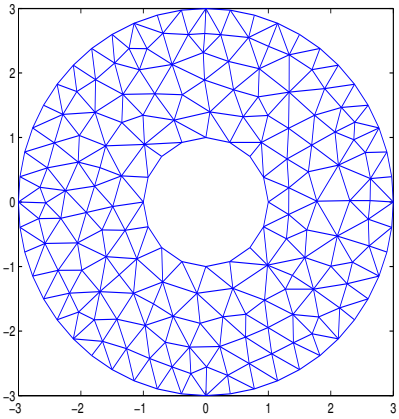

(a) $h = 0.660$

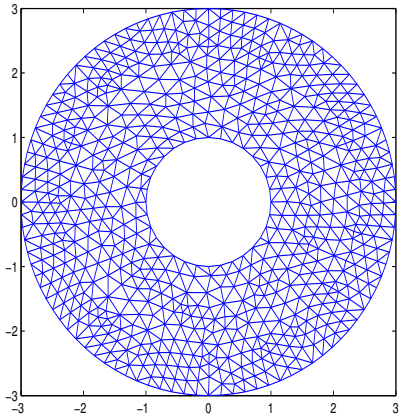

(b) $h = 0.372$

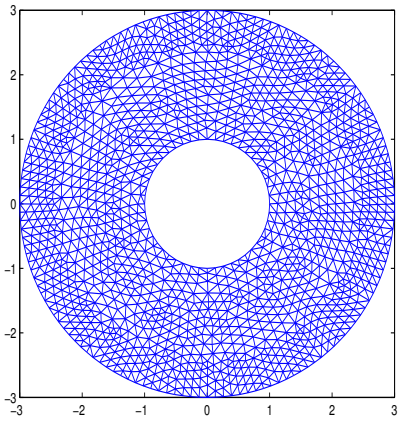

(c) $h = 0.191$

Figure 7: Meshes for the scattering of a metallic cylinder.

References

[ABCM02] D. N. Arnold, F. Brezzi, B. Cockburn, and L. D. Marini, *Unified analysis of discontinuous Galerkin methods for elliptic problems*, SIAM J. Numer. Anal. **39** (2002), no. 5, 1749–1779.

[CFP06] G. Cohen, X. Ferrieres, and S. Pernet, *A spatial high-order hexahedral discontinuous Galerkin*

method to solve Maxwell's equations in time domain, J. Comput. Phys. **217** (2006), no. 2, 340–363.

[CGL09] B. Cockburn, J. Gopalakrishnan, and R. Lazarov, *Unified hybridization of discontinuous Galerkin, mixed, and continuous Galerkin methods for second order elliptic problems*, SIAM J. Numer. Anal. **47** (2009), no. 2, 1319–1365.

[CS89] B. Cockburn and C.-W. Shu, *TVB Runge-Kutta local projection discontinuous Galerkin finite element method for conservation laws II: general framework*, Math. Comp. **52** (1989), 411–435.

[CS98] ———, *The local discontinuous Galerkin method for time-dependent convection-diffusion systems*, SIAM J. Numer. Anal. **35** (1998), no. 6, 2440–2463.

[DFLP08] V. Dolean, H. Fol, S. Lanteri, and R. Perrussel, *Solution of the time-harmonic Maxwell equations using discontinuous Galerkin methods*, J. Comput. Appl. Math. **218** (2008), 435–445.

[Fah10] H. Fahs, *Discontinuous Galerkin method for time-domain electromagnetics on curvilinear domains*, Appl. Math. Sci. **4** (2010), no. 19, 943–958.

[FLLP05] L. Fezoui, S. Lanteri, S. Lohrengel, and S. Piperno, *Convergence and stability of a discontinuous Galerkin time-domain method for the 3d heterogeneous Maxwell equations on unstructured meshes*, ESAIM: Math. Model. and Numer. Anal. **39** (2005), no. 6, 1149–1176.

[FW09] X. Feng and H. Wu, *Discontinuous Galerkin method for Helmholtz equation with large wave numbers*, SIAM J. Numer. Anal. **47** (2009), no. 4, 2872–2896.

[FX11] X. Feng and Y. Xing, *Absolutely stable local discontinuous Galerkin methods for the helmholtz equation with large wave number*, Math. Comp. (2011), submitted.

[GM11] R. Griesmaier and P. Monk, *Error analysis for a hybridizable discontinuous Galerkin method for the Helmholtz equation*, DOI: 10.1007/s10915-011-9460-z, 2011.

[HPS04] P. Houston, I. Perugia, and A. Schotzau, *Mixed discontinuous Galerkin appproximation of the Maxwell's equations*, SIAM J. Numer. Anal. **42** (2004), no. 1, 434–459.

[HPSS05] P. Houston, I. Perugia, A. Schneebeli, and A. Schotzau, *Interior penalty method for the indefinite time-harmonic Maxwell's equations*, Numer. Math. **100** (2005), 485–518.

[HW02] J. S. Hesthaven and T. Warburton, *Nodal high-order methods on unstructured grids: I. time-domain solution of maxwell's equations*, J. Comput. Phys. **181** (2002), no. 1, 186–221.

[HW08] ———, *Nodal discontinuous Galerkin methods - algorithms, analysis, and applications*, Springer, New York, 2008.

[KSC10] R.M. Kirby, S.J. Sherwin, and B. Cockburn, *To CG or to HDG: A comparative study*, Unpublished, 2010.

[NPC09a] N.C. Nguyen, J. Peraire, and B. Cockburn, *An implicit high-order hybridizable discontinuous Galerkin method for linear convection-diffusion equations*, J. Comput. Phys. **228** (2009), no. 9, 3232–3254.

[NPC09b] ———, *An implicit high-order hybridizable discontinuous Galerkin method for nonlinear convection-diffusion equations*, J. Comput. Phys. **228** (2009), no. 23, 8841–8855.

[NPC11] ———, *Hybridizable discontinuous Galerkin methods*, Spectral and high order methods for partial differential equations. Lecture notes in Computational Science and Engineering **76** (2011), 63–84.

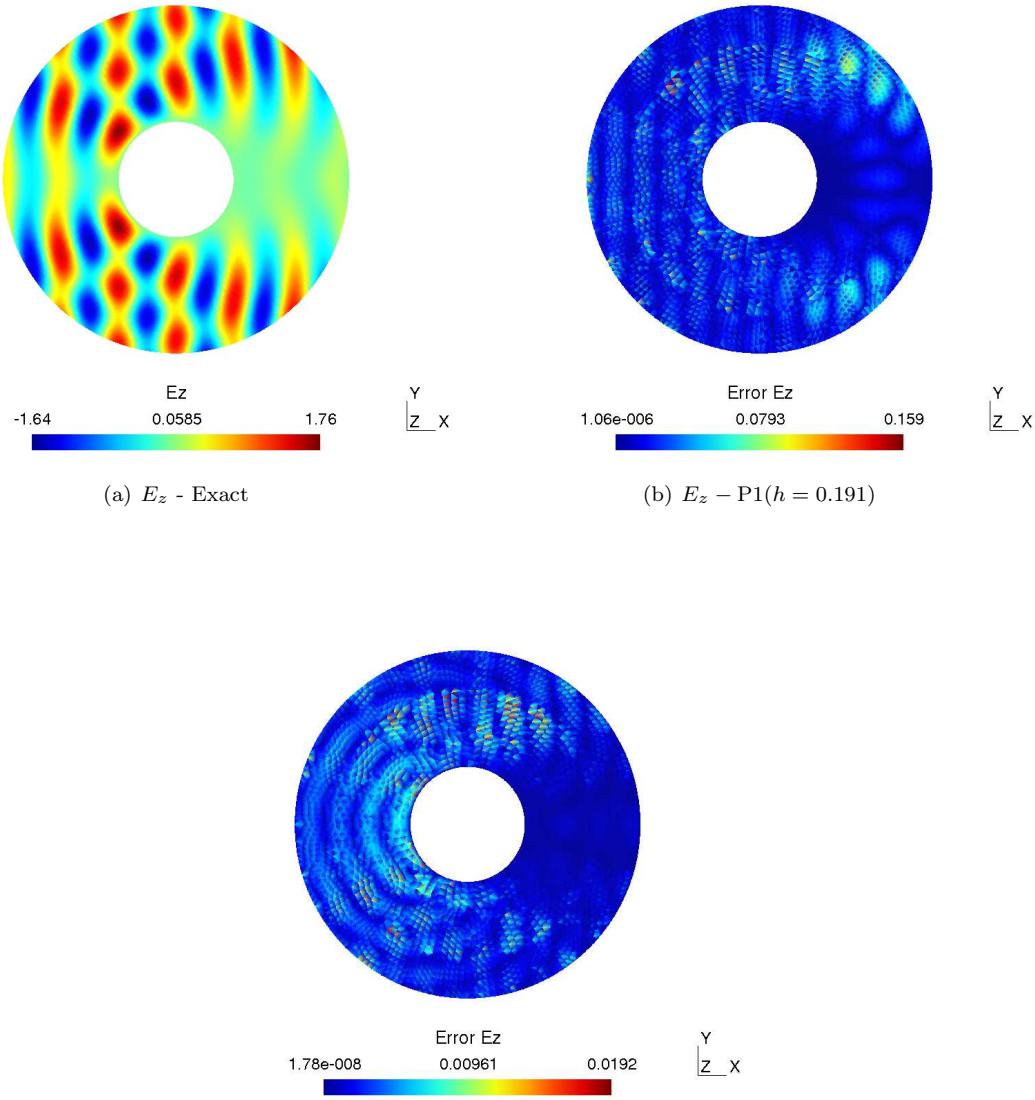

(a) E_z - Exact

(b) $E_z - \mathrm{P1}(h = 0.191)$

(c) $E_z - \mathrm{P2}(h = 0.191)$

Figure 8: Contour lines of the fields and the errors.

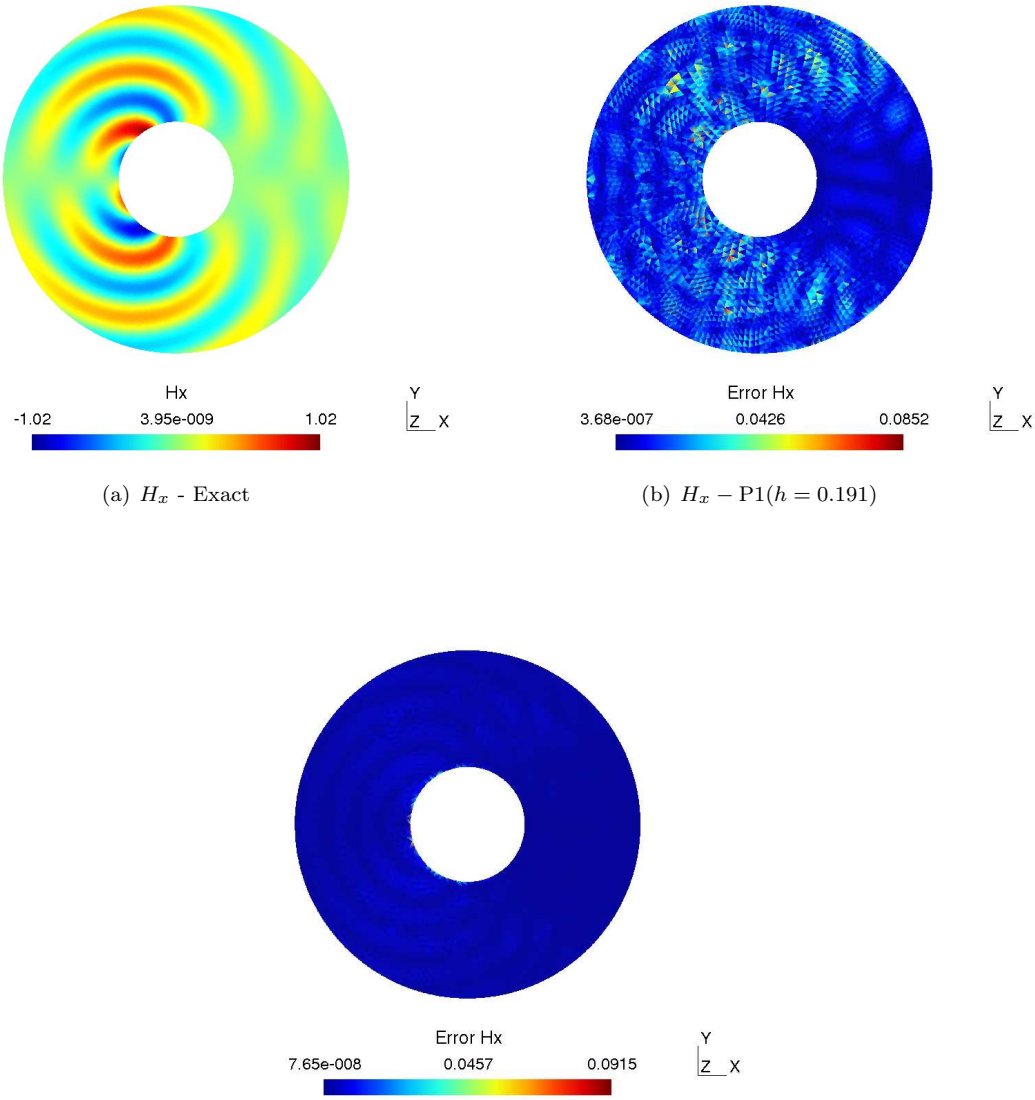

(a) H_x - Exact

(b) $H_x - \mathrm{P1}(h = 0.191)$

(c) $H_x - \mathrm{P2}(h = 0.191)$

Figure 9: Contour lines of the fields and the errors.

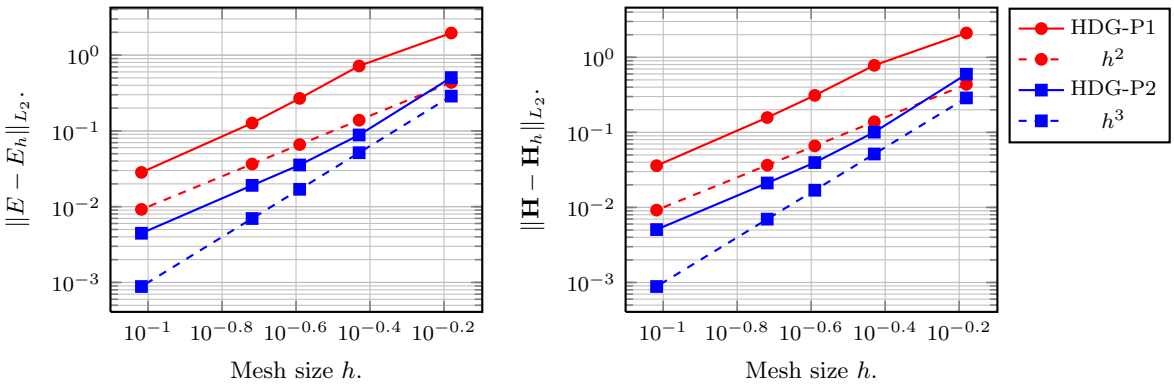

Figure 10: Convergence results for the scattering problem.

Contents

Centre de recherche INRIA Sophia Antipolis – Méditerranée
2004, route des Lucioles - BP 93 - 06902 Sophia Antipolis Cedex (France)

Centre de recherche INRIA Bordeaux – Sud Ouest : Domaine Universitaire - 351, cours de la Libération - 33405 Talence Cedex
Centre de recherche INRIA Grenoble – Rhône-Alpes : 655, avenue de l'Europe - 38334 Montbonnot Saint-Ismier
Centre de recherche INRIA Lille – Nord Europe : Parc Scientifique de la Haute Borne - 40, avenue Halley - 59650 Villeneuve d'Ascq
Centre de recherche INRIA Nancy – Grand Est : LORIA, Technopôle de Nancy-Brabois - Campus scientifique
615, rue du Jardin Botanique - BP 101 - 54602 Villers-lès-Nancy Cedex
Centre de recherche INRIA Paris – Rocquencourt : Domaine de Voluceau - Rocquencourt - BP 105 - 78153 Le Chesnay Cedex
Centre de recherche INRIA Rennes – Bretagne Atlantique : IRISA, Campus universitaire de Beaulieu - 35042 Rennes Cedex
Centre de recherche INRIA Saclay – Île-de-France : Parc Orsay Université - ZAC des Vignes : 4, rue Jacques Monod - 91893 Orsay Cedex

Éditeur
INRIA - Domaine de Voluceau - Rocquencourt, BP 105 - 78153 Le Chesnay Cedex (France)
http://www.inria.fr
ISSN 0249-6399